Three-Dimensional a-Si:H Solar Cells on Glass Nanocone Arrays Patterned by Self-Assembled Sn Nanospheres

Jeehwan Kim,* Augustin J. Hong, Jae-Woong Nah,* Byungha Shin, Frances M. Ross, and Devendra K. Sadana

IBM T.J. Watson Research Center, Yorktown Heights, New York 10598, United States

ABSTRACT

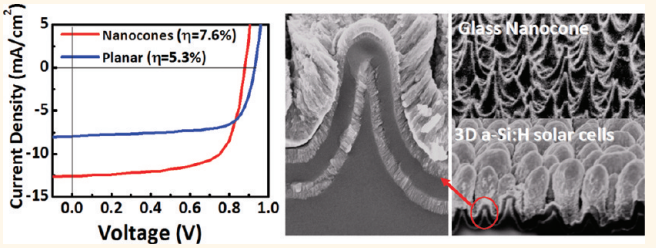

We introduce a cost-effective method of forming size-tunable arrays of nanocones to act as a three-dimensional (3D) substrate for hydrogenated amorphous silicon (a-Si:H) solar cells. The method is based on self-assembled tin nanospheres with sizes in the range of 20 nm to 1.2 μm. By depositing these spheres on glass substrates and using them as an etch mask, we demonstrate the formation of glass nanopillars or nanocones, depending on process conditions. After deposition of 150 nm thick a-Si:H solar cell p-i-n stacks on the glass nanocones, we show an output efficiency of 7.6% with a record fill factor of ~69% for a nanopillar-based 3D solar cell. This represents up to 40% enhanced efficiency compared to planar solar cells and, to the best of our knowledge, is the first demonstration of nanostructured p-i-n a-Si:H solar cells on glass that is textured without optical lithography patterning methods.

KEYWORDS: a-Si:H solar cells · self-assembled tin nanospheres · nanopillars · nanocones · three-dimensional solar cells

Vertical nanopillar (NP) solar cells are of great interest because they would allow for ultimate light trapping and excellent charge separation. They could therefore achieve potentially higher efficiency than thin film planar cells, with the added merits of minimal use of materials and much lower process cost.[1−6] However, NP fabrication for solar cells has quite stringent requirements when compared to fabrication for nanoscale electronics and optoelectronics. These requirements include (i) cost-effectiveness of the nanopatterning process for fulfilling the less than a dollar per watt criterion; (ii) a "nano" pillar diameter in the range of hundreds of nanometers for maximizing light trapping; and (iii) a low-temperature process to prevent deformation of inexpensive substrates such as glasses and polymers. Popular methods for the fabrication of NP solar cells have included both bottom-up techniques, such as vapor−liquid−solid (VLS) growth,[4,5] and top-down patterning, through polymer or silica nanosphere masks,[1,2] other masks formed by self-assembly processes,[7,8] or lithography.[9−11] VLS growth is an excellent method to form NP solar cells. However, it requires single-crystal silicon (c-Si) ⟨111⟩ layer transfer and photolithographic methods to form the metal catalysts, both increasing the process cost. Furthermore, the VLS growth temperature is relatively high (>800 °C), which makes it incompatible with many glass and polymer materials. One top-down approach to form NPs is to coat a substrate with polymer or glass nanobeads that act as etch masks.[1,2] Nanobead synthesis may increase process cost, and furthermore, such materials are not desirable in patterning glass substrates due to their low etch selectivity compared to metallic materials. A self-masked dry etching technique may be a simpler top-down NP formation approach,[7,8] using, for example, a reactive gas mix that forms SiC nanoparticles on a Si substrate which then act as an etch mask. Although such self-masking has been demonstrated for c-Si substrates, a similar principle could be used to pattern glass substrates by modifying the chemistry and plasma. Nanoimprint lithography and nanomolding have recently been introduced for nanopattern transfer for photovoltaic (PV) fabrication.[9−11] They have worked successfully at relatively low temperatures but require multiple process steps, which may increase manufacturing cost.

In this paper, we propose a photolithography-free nanopatterning method that meets the above three requirements, making it well-suited for PV applications.

* Address correspondence to jeehwkim@us.ibm.com, jnah@us.ibm.com.

Received for review September 14, 2011 and accepted December 8, 2011.

Published online December 08, 2011
10.1021/nn203536x

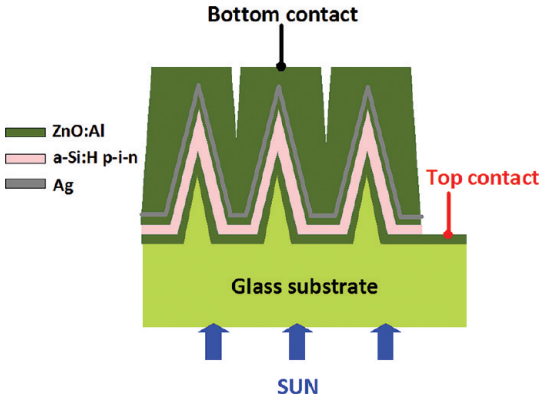

Figure 1. Schematic of the 3D a-Si:H solar cell fabricated on glass NCs.

The method is based on the use of tin (Sn) nanospheres, which self-assemble during rapid thermal annealing (RTA) of Sn films on glass substrates and show great size tunability from tens of nanometers to micrometers. This is a low-temperature process, due to the low melting point of Sn (232 °C), allowing great freedom for choosing substrates that cost less than Si. We will show that slow morphological changes of Sn nanoparticles due to Sn oxidation allow a very high density of nanospheres to form during annealing. We can therefore form dense arrays of Sn nanospheres with diameters in the hundreds of nanometer range on glass substrates, then use them as an etch mask for deep reactive ion etching (DRIE) to form NPs. Finally, we use chemical etching to taper the NPs into glass nanocones (NCs). These NCs are not themselves used as the active PV materials, but instead are used as building blocks for three-dimensional (3D) thin film hydrogenated amorphous Si (a-Si:H) solar cells. The device structure is shown schematically in Figure 1: aluminum-doped zinc oxide (ZnO:Al) is deposited on top of the glass NCs as a front electrode, followed by 150 nm thick single junction a-Si:H p-i-n stacks. We will show up to 40% enhancement on conversion efficiency from these 3D a-Si:H solar cells, compared to planar cells at the same absorber thickness. We will show that the enhancement is mainly due to enhanced short circuit current, and we will also show a surprisingly high (record) fill factor of ~69% from the same single junction device. To the best of our knowledge, this is the first demonstration of a high-performance lithography-free 3D a-Si:H solar cell on a glass NCs.

RESULTS AND DISCUSSION

Formation of Self-Assembled Sn Nanosphere and Hemisphere Arrays. Sn solders are used at length scales of hundreds of micrometers in joining techniques to form ball grid arrays on copper at the back end of the line in a complementary metal-oxide-semiconductor process.[12−14] Since Sn-based materials have a strong tendency to be oxidized, a strong antioxidizer, or "flux", is applied to the Sn to make it dewet from the substrate and transform into spheres (spheroidization) upon annealing around 250 °C.[12−14] The flux is typically composed of diethylene triamine pentaacetic acid, tetrakisethylenediamine, and glycerol ethoxylate, which together mechanically crack the surface Sn oxide and inhibit the Sn surface from subsequent oxidation. On a nonwetting surface, this results in the formation of complete Sn spheres upon melting.[15]

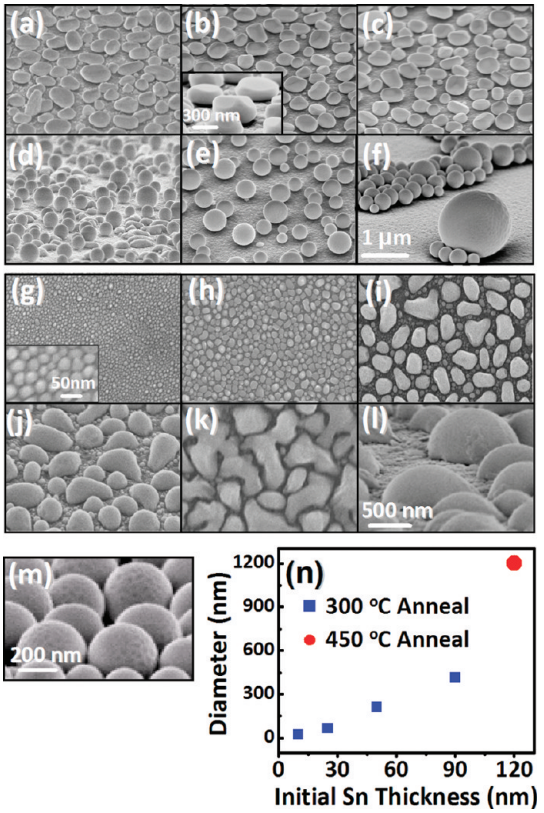

Figure 2. Morphology of Sn nanoparticle arrays with different thicknesses, annealing temperatures, and oxidation conditions: (a−f) 90 nm thick Sn films with flux, annealed for 10 s at 150, 200, 220, 230, 250, and 300 °C, respectively; (g−k) 10, 25, 50, 90, and 100 nm thick Sn films, respectively, with no flux, annealed at 300 °C; (l) 120 nm thick Sn film with no flux, annealed at 450 °C; (m) magnified view of (f) to highlight the facets seen on the surface of the Sn spheres after cooling. (n) Average diameter of hemispheres in (g−l) as a function of Sn thickness.

For our experiments, we require Sn structures in the tens of nanometers to micrometer range. It is not possible to form spheres out of micrometer thickness Sn layers without applying flux because the Sn oxide surface layer significantly slows diffusion of Sn atoms, preventing rearrangement into the equilibrium shape.[12−14] We therefore formed Sn nanospheres by first depositing 10−120 nm thick Sn films on glass substrates using thermal evaporation at room temperature. We then heated the films in a rapid thermal annealing (RTA) furnace under a N_2 flow at temperatures from 150 to 450 °C for 10 s using flux and compared with the same anneal without flux. It is well-known that Sn does not wet the glass surface

and does not intermix with SiO_2.[16] Therefore, it can be expected that the interfacial energy of Sn/SiO_2 is so great that there is a strong tendency for spheroidization of thin film Sn deposited on glass.

Figure 2a–f shows the resulting morphologies for flux-coated 90 nm thick Sn films after 10 s of RTA at various temperatures from 150 to 300 °C. An abrupt morphological change in the Sn particles is evident at 230 °C, the melting temperature of Sn. Spheres form above the melting point (Figure 2e,f), while lens-like particles form below the melting point (Figure 2a–c). Near the melting point, spheres and partially spheroidized hemispheres (lenses) coexist (Figure 2d). Over the entire temperature range, Sn particles do not appear to wet the glass surface, implying that the interfacial energies of both solid Sn/glass and liquid Sn/glass are too high for Sn to form a continuous film on the glass surface. We expect that the activation energy for diffusion in the liquid is significantly lower than that in the solid due to the lower bonding energy of atoms in the liquid.[17] Thus, the different morphologies for solid and liquid particles suggest that a kinetic limitation at temperatures below the melting point prevents the solid Sn particles from rearranging into spheres to minimize the surface area. Instead, solid state diffusion appears to favor the formation of a lens-like morphology with surface facets, where lower surface energy lattice planes are exposed to the vapor. Even the complete spheres show small facets after cooling (Figure 2m), similar to those observed in other metal systems.[18,19] Precise analysis of the crystallographic orientations could be followed in future work.

While the lens-like morphologies obtained below the melting temperature show a relatively uniform size distribution, aggressive morphological evolution takes place in the liquid Sn at higher temperatures. Particle coarsening is evident, as manifested by the nonuniform distribution of sphere sizes. This becomes most prominent at 300 °C, well above the melting temperature, with a large variation in particle size visible in Figure 2f.

Isothermal anneals result in a similar morphological evolution, from the two-dimensional film to lens-like shapes, which then transform into spheres showing a broader size range (Figure 3a). It is noteworthy that Sn lenses were obtained even at 150 °C, well below the melting temperature. This morphology has not been observed for micrometer scale solder balls.[12–14] We believe that it is technologically significant that one can achieve nanoscale templates at such low temperatures, implying great flexibility in choosing polymer and glass substrates for further patterning processes.

When flux was not applied to the Sn surface, RTA temperatures slightly above the melting point do not result in the ball-up of nanometer scale Sn films (not shown). This is consistent with the behavior observed

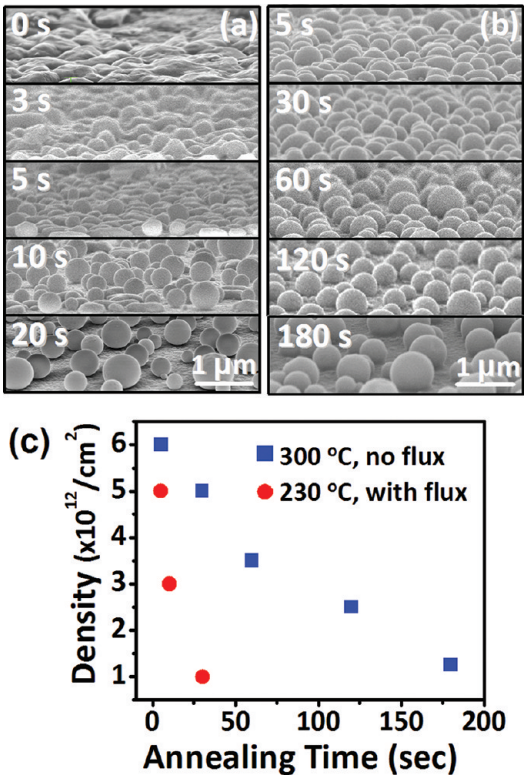

Figure 3. Morphological change of Sn nanoparticles as a function of the isothermal RTA times indicated: (a) 90 nm thick Sn films annealed at 230 °C with flux; (b) 90 nm thick Sn films annealed at 300 °C without flux; (c) average Sn particle density as a function of annealing time with and without flux.

for micrometer scale Sn-based solders, in that the Sn layer cannot be agglomerated without applying a flux.[12–14] However, supplying further thermal energy to the nanometer scale Sn films by an RTA well above the melting point, for 10 s under a N_2 ambient at 300 °C, leads to the formation of Sn hemispheres, even without flux (Figure 2g–k). Complete spheroidization was not observed for that short annealing time. The annealing ambient does not seem to affect the results, whether it is a hot plate anneal in air, RTA in N_2, or even annealing at a vacuum level of 1×10^{-5} Torr. This is presumably due to the high oxidation rate of the Sn surface without flux,[20] and it appears that ultrahigh vacuum conditions would be necessary for full control of the Sn surface oxidation.

In order to explore the range of sizes available from this nanopatterning technique, we examined the effect of Sn film thickness over the range of 10–120 nm, without flux and for an RTA at 300 °C for 10 s. Results are shown in Figure 2g–k. Dense arrays of hemispherical Sn particles were formed for Sn films thinner than 100 nm (Figure 2g–j). Interestingly, above 100 nm, hemispheres do not form (Figure 2k), which suggests that higher temperatures or longer times are required. Hemispheres are in fact obtained for 120 nm thick Sn films when annealed at a higher temperature of 450 °C

(Figure 2l). The size range of the self-assembled Sn hemispheres is quantified in Figure 2n. A monotonic increase in an average diameter is observed from 20 to 400 nm, as the thickness of a 300 °C annealed Sn film increases, and larger particle sizes of 1.2 μm can be obtained with thicker Sn films and higher annealing temperatures. Thus, we can obtain hemispheres at high density with diameters ranging from 20 nm to 1.2 μm by appropriate choice of deposition and annealing parameters. In contrast, VLS NPs grown from Au particles that are formed by agglomerating (thinner) Au films have a lower density, especially after coarsening to increase the Au size.[21] Additionally, the broad range of feature sizes offered by Sn is in contrast to the 10−50 nm nanodomains routinely obtained by block copolymers.[22]

Control of the morphology between hemispheres and spheres is possible by additional annealing. The morphological evolution of Sn hemispheres with annealing time is shown in Figure 3b at a fixed temperature of 300 °C and with an initial film thickness of 90 nm. The hemispherical Sn nanoparticles tend to dewet the glass surface as the annealing time increases. Dewetting (*i.e.*, a wetting angle larger than 90°) becomes clear after 60 s, and spheres were eventually formed after 3 min of annealing. In contrast, for flux-coated Sn particles, only 10 s RTA at 230 °C is required to form complete spheres (Figure 3a). The faster oxidation rate of Sn without flux is primarily responsible for the slowing of the morphological evolution because Sn oxide acts as a diffusion barrier for Sn atoms.[12,13,20] As shown in Figure 3c, particle densities are significantly reduced as the annealing time increases because of particle coarsening, and the rate of density decrease is clearly faster for the flux-coated samples, even at the lower annealing temperatures, because of enhanced Sn diffusion. Regardless of whether flux is applied, the nonwettability of Sn on glass is confirmed by these experiments. The slow morphological evolution rate obtained without flux offers particularly good control over the morphologies of the Sn nanopatterns and allows excellent choice of the Sn nanosphere density.

Formation of Glass NPs and NCs. The great flexibility in forming different nanotemplates described above allows us to fabricate glass NPs with a variety of sizes and shapes. We achieve this by performing DRIE on the glass substrates through the Sn patterns. We aimed at obtaining templates with diameters in the hundreds of nanometer range as cost-effective building blocks for nanostructured thin film a-Si:H solar cells with high light trapping capability.[3,6] Several glass NP templates are shown in Figure 4d−f and were formed *via* DRIE through the mask patterns in Figure 4a−c, respectively.

DRIE first forms NPs, but glass NPs themselves cannot be used as the templates for subsequently

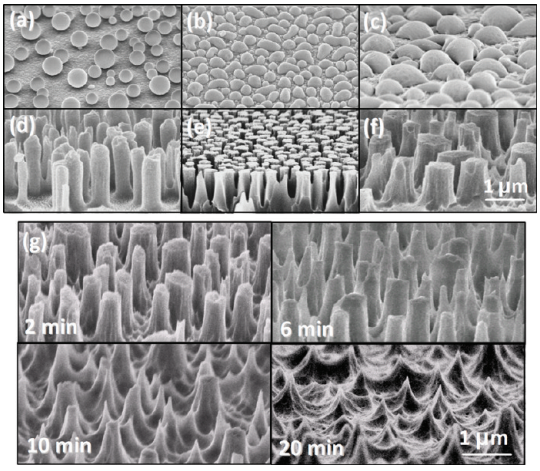

Figure 4. Morphology of NPs and NCs formed from different templates. (a−c) Sn particle masks formed by annealing (a) 90 nm thick Sn films with flux at 250 °C, (b) 90 nm thick Sn films without flux at 300 °C, and (c) 120 nm thick Sn films without flux at 450 °C. (d−f) NPs formed by DRIE of glass substrates through the masks in (a−c), respectively. DRIE was performed in 100 mTorr CF_4 gas flow and a power density of 425 mW/cm^2 for 30 min. (g) Morphology change from columns to cones formed by 45 min DRIE of (c) followed by wet chemical etching for the times indicated using 50:1 diluted HF.

grown ZnO:Al electrodes and a-Si:H p-i-n stacks. This is because these layers are deposited through plasma processes which are known to be nonconformal and would therefore result in thicker layers on the top of the NPs compared to the side walls. Instead, a conical shape is more desirable with tapered tops for the pillars. Cones are also more beneficial than pillars in terms of light trapping capability.[23] We therefore tapered the glass NPs after DRIE by isotropic wet chemical etching using a diluted HF dip. Typically, Sn hemispheres remain on top of the NPs directly after the DRIE step, but they are automatically removed during the HF tapering process. As shown in Figure 4g, as etching takes place, the top diameter of the NPs tapers to result in NCs.

3D a-Si:H Solar Cell Fabrication on Glass NCs. 3D c-Si NP solar cells have already been clearly demonstrated by several studies.[1,2,4,5] For example, c-Si NP p−n junction solar cells formed on c-Si substrates etched through silica nanosphere masks show efficiencies above 5% and fill factors (FF) ~55%,[1,2] while c-Si NP p−n junction solar cells based on VLS NPs show conversion efficiencies up to 7.9% with FF 65%.[4] However, c-Si NP solar cells whose efficiency exceeds that of planar control cells have apparently not yet been demonstrated. This is mainly due to the poor FF of the c-Si NP solar cells (by comparison, the typically reported FF of c-Si planar solar cells is ~80%[24]). This reduction in FF is considered to be a result of the increased surface area of the active PV materials, combined with improper surface passivation.[5] To avoid these issues, instead of using NPs as PV active materials, we therefore propose to use

the glass NCs described above as templates for subsequent fabrication of 3D thin film a-Si:H solar cells. The structure of 3D a-Si:H p-i-n cells on NCs, where the NCs serve only as templates to deposit the a-Si:H, has two advantages over c-Si NP solar cells: the surface of the a-Si:H film itself is already completely passivated by hydrogenation, and generated carriers can be collected more efficiently with p-i-n rather than p−n configurations.[25] The a-Si:H on NC concept has already been proven to work by Naughton *et al.*,[6] by forming n-i-p a-Si:H stacks on lithographically patterned c-Si NC templates coated with metal contacts (Ag−Au−Ti). Although these structures used an expensive c-Si substrate and an n-i-p configuration which is undesirable for manufacturing (see below), they demonstrated a remarkable efficiency of 8% and a FF of 65%. Considering that the typically reported FF of a-Si:H single junction cells is ~70%,[25] this is a significant accomplishment. For a-Si:H solar cell technology, the "superstrate" configuration, with p-i-n layers on a glass substrate coated with transparent conducting oxide, is more commonly used than the n-i-p on metal (substrate) configuration, as employed by Naughton *et al.*[6] This is because a superstrate configuration is fully compatible with laser-scribing for monolithic module integration and already provides effective encapsulation of the front of the cells.[26] The superstrate configuration has recently been used to demonstrate 10.3% efficient a-Si:H/μc-Si:H tandem cells on nanostructured ZnO:Al,[27] lithographically fabricating an inverse form of ZnO:Al NPs (Swiss cheese ZnO:Al) on glass substrates. Nonlithographic superstrate configurations remain to be demonstrated.

We show below our superstrate demonstration of 3D a-Si:H p-i-n stacks on NC textured glass substrates, formed by self-assembly without costly or complex patterning. Figure 5a shows the starting glass NCs, and Figure 5b,c shows the finished 3D a-Si:H solar cell stacks on glass NCs. The PV films were deposited in the following sequence: (i) 120 nm ZnO:Al as a front contact, (ii) 10 nm p^+ μc-SiC:H, (iii) 130 nm intrinsic a-Si:H, (iv) 10 nm n^+ a-Si:H, (v) 120 nm ZnO:Al/50 nm Ag to act as a back-reflector as well as a bottom contact, and (vi) 2 μm ZnO:Al as a protection layer. The quoted thicknesses were measured from the side wall of the NCs. We find that deposition of the 2 μm ZnO:Al protection layer to completely fill the gaps between the NC solar cells is helpful for mechanical strength since the probes used for measurements tend to break freestanding NCs.

The *J*−*V* characteristics of the finished cells were measured under 1 sun illumination of the glass substrates. The measured *J*−*V* curves and solar cell parameters are shown in Figure 5d and Table 1, respectively. As a control, p-i-n stacks with thicknesses of 200 and 150 nm were deposited on untextured planar ZnO:Al films on glass substrates (200 and

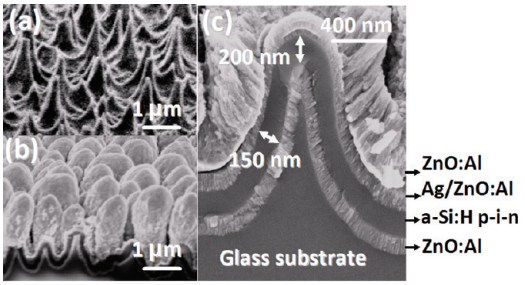

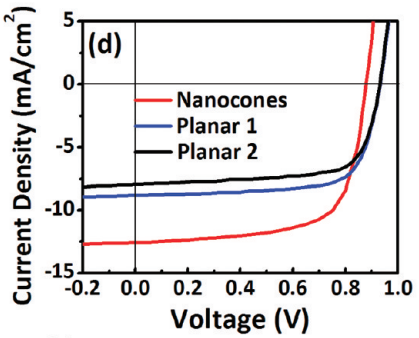

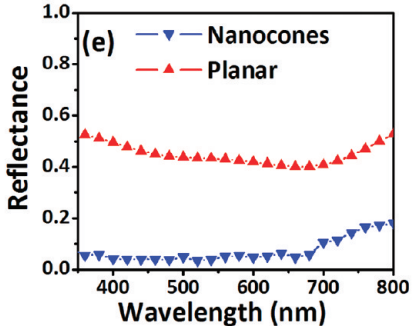

Figure 5. (a) Glass NC template formed under the conditions shown in Figure 4g with 10 min etching; (b) full a-Si:H solar cell stack; (c) single glass NC showing the full a-Si:H solar cell stack in cross section. (d) *J*−*V* curves of a-Si:H single junction solar cells on glass NCs and on planar substrates coated with ZnO:Al front electrodes. (e) Reflectance of a-Si:H films on glass NCs and planar substrates.

TABLE 1. Parameters of a-Si:H Single Junction Solar Cells on Glass NCs and on Planar Substrates Coated with ZnO:Al Front Electrodes

cell type	efficiency (%)	FF (%)	J_{SC} (mA/cm^2)	V_{OC} (mV)
nanocones	7.6	69	12.6	879
planar 1	5.9	71	8.8	932
planar 2	5.3	72	8.0	931

150 nm thick planar cells are indicated as "planar 1" and "planar 2", respectively, in Figure 5d and Table 1). These thicknesses were chosen to encompass the thickness variation of the 3D a-Si:H p-i-n layer, from 150 nm at the side wall to 200 nm at the NC tips (with the fraction of side wall areas obviously significantly higher than tip areas). Figure 5d compares the *J*−*V* of samples with and without NCs. Short circuit currents (J_{SC}) obtained from the 150 and 200 nm thick planar cells are 8.0 and 8.8 mA/cm^2, respectively, whereas that from the 150 nm NC cells is 12.6 mA/cm^2. Compared to

planar solar cells, a substantial efficiency enhancement of up to 40% was obtained. The efficiency enhancement is due to a ~50% increase in J_{SC}, even though the open circuit voltage (V_{OC}) of the NC solar cells is reduced by up to ~10%. We attribute the J_{SC} increase to enhanced light absorption at the NC solar cells, as supported by the near-zero reflectance measured from NCs and shown in Figure 5e, as well as an increased volume of absorbers per unit area. (Under the assumption that cones are closely packed and have an aspect ratio of 1.5:1, the volume of absorbers on the NC substrates is approximately 3.4 times greater than that on planar substrates.) This is a substantial improvement even compared to solar cells on conventional textured transparent conducting oxides such as APCVD SnO:F and LPCVD ZnO:B, where 25−35% J_{SC} enhancement has been obtained.[11,28] A surprisingly high FF of 69% was measured, which is close to that obtained from planar solar cells. A similar shunt resistance was obtained for both planar and NC cells, showing the similar slopes of the $J-V$ curves at J_{SC}. When compared to the 65% FF obtained in the substrate configuration,[6] we suggest that the improved superstrate FF here is due to a reduced shunt rather than a reduced series resistance. We believe that p-i-n deposition on ZnO:Al, as used here, could reduce the chance of cell contamination from the Ag−Au−Ti contacts as used in the substrate configuration.[6] Compared to the FF obtained from c-Si NP solar cells, the higher value obtained here reflects the inherent hydrogen passivation of the a-Si:H surface. Finally, we note that this is the first demonstration of highly performing a-Si:H p-i-n cells on litho-free nanostructures, to our knowledge. This result could imply that the benefit from using 3D structures will be greater for a-Si:H materials compared to c-Si materials.

We expect that increasing the thickness of the p-i-n stacks, if the same ~40% enhancement over planar cells could be maintained, would lead to record a-Si:H solar cell efficiencies. However, the diameter (<1 μm) of the glass NCs used in this study is too small to accommodate thicker PV stacks. For further improvement in efficiency, therefore, it is worthwhile to increase the cone diameter to over a micrometer and correspondingly increase the distance between cone tips by optimizing the initial Sn deposition and annealing conditions.

CONCLUSIONS

We have demonstrated 3D a-Si:H solar cells on glass NCs that were fabricated from glass substrates patterned *via* self-assembled Sn nanosphere masks. Dense Sn patterns with sizes ranging from tens of nanometers to a micrometer could be obtained on glass, depending on process conditions, with Sn in the form of either spheres or hemispheres. DRIE through the hemisphere masks results in the formation of glass NPs, and subsequent wet chemical tapering forms glass NCs. Three-dimensional a-Si:H solar cells created on NC patterned substrates showed record FFs of 69% and substantial efficiency improvements of up to 40% compared to planar solar cells. These results clearly show the beneficial effects of nanostructuring for efficiency enhancement of solar cells. Although the 3D solar cells have so far been limited to a-Si:H based materials, the patterning method described here could be applied to other PV materials, potentially achieving improved performance through low-cost processing steps.

METHODS

Sn Nanosphere Formation. Sn was deposited in a thermal evaporator at a vacuum level of 5×10^{-5} Torr with thicknesses ranging from 10 to 120 nm on borofloat glass substrates using a deposition rate of 0.5 nm/s. To form pure SiO_2 layers, 2 μm thick SiO_2 was deposited on the borofloat glass substrates using plasma-enhanced chemical vapor deposition (PECVD). In order to form nanospheres, 10% flux diluted in isopropyl alcohol was spin-coated on the Sn surface at 3000 rpm. Annealing was then performed in a RTA chamber under a N_2 flowing ambient. For nanohemisphere formation, as-deposited Sn films were loaded into the RTA chamber immediately after thermal evaporation and annealed.

Glass NP and NC Formation. After forming the desired Sn nanopatterns, DRIE was performed in a 100 mTorr CF_4 gas flow using a power density of 425 mW/cm^2. This DRIE process results in the formation of glass NPs. Subsequent dipping into 50:1 diluted HF solution tapers the top ends of the pillars leading to formation of glass NCs.

a-Si:H Solar Cell Fabrication. a-Si:H solar cells were fabricated on glass NCs by depositing boron and carbon-doped p^+ (window layer) μc-SiC:H, undoped instrinsic a-Si:H (absorber layer), and phosphorus-doped n^+ a-Si:H, at 250 °C in a PECVD chamber with the following thicknesses: 10 nm p^+, 130 nm i, and 10 nm n^+.

REFERENCES AND NOTES

1. Garnett, E.; Yang, P. Light Trapping in Silicon Nanowire Solar Cells. *Nano Lett.* **2010**, *10*, 1082–1087.
2. Garnett, E.; Yang, P. Silicon Nanowire Radial p−n Junction Solar Cells. *J. Am. Chem. Soc.* **2008**, *130*, 9224–9225.
3. Kelzenberg, M. D.; Boettcher, S. W.; Petykiewicz, J. A.; Turner-Evans, D. B.; Putnam, M. C.; Warren, E. L.; Spurgeon, J. M.; Briggs, R. M.; Lewis, N. S.; Atwater, H. A. Enhanced Absorption and Carrier Collection in Si Wire Arrays for Photovoltaic Applications. *Nat. Mater.* **2010**, *9*, 239–244.
4. Putnam, M. C.; Boettcher, S. W.; Kelzenberg, M. D.; Turner-Evans, D. B.; Spurgeon, J. M.; Warren, E. L.; Briggs, R. M.; Lewis, N. S.; Atwater, H. A. Si Microwire-Array Solar Cells. *Energy Environ. Sci.* **2010**, *3*, 1037–1041.
5. Gunawan, O.; Guha, S. Characteristics of Vapor−Liquid−Solid Grown Silicon Nanowire Solar Cells. *Sol. Energy Mater. Sol. Cells* **2009**, *93*, 1388–1393.
6. Naughton, M. J.; Kempa, K.; Ren, Z. F.; Gao, Y.; Rybczynski, J.; Argenti, N.; Gao, W.; Wang, Y.; Peng, Y.; Naughton, J. R.; *et al.* Efficient Nanocoax-Based Solar Cells. *Phys. Status Solidi* **2010**, *R4*, 181–183.
7. Huang, Y. F.; Chattopadhyay, S.; Jen, Y. J.; Peng, C. Y.; Liu, T. A; Hsu, Y.; Pan, C. L.; Lo, H. C.; Hsu, C. H.; Chang, Y. H.; *et al.* Improved Broadband and Quasiomnidirectional Anti-reflection Properties with Biomimetic Silicon Nanostructures. *Nat. Nanotechnol.* **2007**, *2*, 770–774.
8. Hsu, C. H.; Lo, H. C.; Chen, C. F.; Wu, C. T.; Hwang, J. S.; Das, D.; Tsai, J.; Chen, L. C.; Chen, K. H. Generally Applicable Self-Masked Dry Etching Technique for Nanotip Array Fabrication. *Nano Lett.* **2004**, *4*, 471–475.

9. Bass, J. D.; Schaper, C. D.; Rettner, C. T.; Arellano, N.; Alharbi, F. H.; Miller, R. D.; Kim, H. C. Transfer Molding of Nanoscale Oxides Using Water-Soluble Templates. *ACS Nano* **2011**, *5*, 4065–4072.
10. Battaglia, C.; Escarré, J.; Söderström, K.; Erni, L.; Ding, L.; Bugnon, G.; Billet, A.; Boccard, M.; Barraud, L.; Wolf, S. D.; *et al.* Nanoimprint Lithography for High-Efficiency Thin-Film Silicon Solar Cells. *Nano Lett.* **2011**, *11*, 661–665.
11. Battaglia, C.; Escarre, J.; Soderstrom, K.; Charriere, M.; Despeisse, M.; Haug, F.-J.; Ballif, C. Nanomoulding of Transparent Zinc Oxide Electrodes for Efficient Light Trapping in Solar Cells. *Nat. Photonics* **2011**, *5*, 535–538.
12. Puttlitz, J.; Stalter, K. A. *Handbook Of Lead-Free Technology for Microelectronics Assemblies*; Marcel Dekker, Inc.: New York, 2004.
13. Minges, M. L. *Electronic Materials Handbook: Packaging*; ASM International: Washington, DC, 1989.
14. Goldmann, L. S.; Krall, B. Measurement of Solder−Flux−Vapor Surface Tension by a Modified Maximum Bubble Pressure Technique. *Rev. Sci. Instrum.* **1976**, *47*, 324–325.
15. Duchesne, E.; Gaynes, M.; Gosselin, T. A.; Lee, K. W.; Obserson, B. Flux Composition and Techniques for Use Thereof. US. Patent US 7,740,713 B2, 2010.
16. Colaianni, M. L; Chen, P. J.; Yates, J. T. The Sn/SiO_2 Interface-Tin Oxidation in the Presence of Sodium Oxide. *Appl. Surf. Sci.* **1993**, *68*, 467–475.
17. Porter, D. A.; Easterling, K. E. *Phase Transformations in Metals and Alloys*; CRC Press: Boca Raton, FL, 2008.
18. Chatain, D.; Ghetta, V.; Wynblatt, P. Equilibrium Shape of Copper Crystals Grown on Sapphire. *Interface Sci.* **2004**, *12*, 7–18.
19. Bonzel, H. P.; Nowicki, M. Absolute Surface Free Energies of Perfect Low-Index Orientations of Metals and Semiconductors. *Phys. Rev. B* **2004**, *70*, 245430.
20. Boggs, W. E.; Kachik, R. H.; Pellissier, G. E. The Oxidation of Tin. *J. Electrochem. Soc.* **1961**, *108*, 6–12.
21. Hannon, J. B.; Kodambaka, S.; Ross, F. M.; Tromp, R. M. The Influence of the Surface Migration of Gold on the Growth of Silicon Nanowires. *Nature* **2006**, *440*, 69–71.
22. Bang, J.; Jeong, U.; Ryu, D. Y.; Russell, T. P.; Hawker, C. J. Block Copolymer Nanolithography: Translation of Molecular Level Control to Nanoscale Patterns. *Adv. Mater.* **2009**, *21*, 4769–4792.
23. Zhu, J.; Yu, Z.; Burkhard, G. F.; Hsu, C. M.; Connor, S. T.; Xu, Y.; Wang, Q.; McGehee, M.; Fan, S.; Cui, Y. Optical Absorption Enhancement in Amorphous Silicon Nanowire and Nanocone Arrays. *Nano Lett.* **2009**, *9*, 279–282.
24. Green, M. A.; Emery, K.; Hishikawa, Y.; Warta, W. Solar Cell Efficiency Tables (Version 36). *Prog. Photovoltaics* **2010**, *18*, 346–352.
25. Tian, B.; Zheng, X.; Kempa, T. J.; Fang, Y.; Yu, N.; Yu, G.; Huang, J.; Lieber, C. M. Coaxial Silicon Nanowires as Solar Cells and Nanoelectronic Power Sources. *Nature* **2007**, *449*, 885–890.
26. Ellmer, K.; Klein, A.; Rech, B. *Transparent Conductive Zinc Oxide: Basics and Applications in Thin Film Solar Cells*; Springer Series In Materials Science.
27. Vanecek, M.; Babchenko, Q.; Purkrt, A.; Holovsky, J.; Neykova, N.; Poruba, A.; Remes, Z.; Meier, J.; Kroll, U. Nanostructured Three-Dimensional Thin Film Silicon Solar Cells with Very High Efficiency Potential. *Appl. Phys. Lett.* **2011**, *98*, 163503–163505.
28. Meier, J.; Kroll, U.; Dubail, S.; Golay, S.; Fay, S.; Dubail, J.; Shah, A. Efficiency Enhancement of Amorphous Silicon p-i-n Solar Cells by LP-CVD ZnO. *IEEE Photovoltaic Spec. Conf.* **2000**, 746–749.